Optomechanical compensatory cooling mechanism with exceptional points

Guo-Qing Qin,[1,*] Xuan Mao,[2,*] Hao Zhang,[3] Peng-Yu Wen,[2] Gui-Qin Li,[2,4] Dong Ruan,[2,4] and Gui-Lu Long[2,4,5,†]

[1]*Beijing Institute of Radio Measurement, The Second Academy of China Aerospace Science and Industry Corporation (CASIC), Beijing 100854, China*

[2]*Department of Physics, State Key Laboratory of Low-Dimensional Quantum Physics, Tsinghua University, Beijing 100084, China*

[3]*Purple Mountain Laboratories, Nanjing 211111, China*

[4]*Frontier Science Center for Quantum Information, Beijing 100084, China*

[5]*Beijing Academy of Quantum Information Sciences, Beijing 100193, China*

(Received 7 September 2022; accepted 6 December 2022; published 22 December 2022)

The ground-state cooling of the Brillouin scattering optomechanical system is limited by defects in practical samples. In this paper, we present a compensatory cooling mechanism for a Brillouin scattering optomechanical system with exceptional points (EPs). The dual-EP system, described in this paper, can be induced by two defects with specific relative angles and is demonstrated to effectively compensate the limited cooling process. The system actively manipulates the coupling strength of not only the optical modes but also the Brillouin phonon modes. Our results provide tools to manipulate the optomechanical interaction in multimode systems and open possibilities for quantum state transfer and quantum interface protocols based on phonon cooling in quantum applications.

DOI: 10.1103/PhysRevA.106.063510

I. INTRODUCTION

Coherent control of the interaction between light and matter is at the heart of quantum technology and fundamental studies. Cavity optomechanics [1], which takes advantage of an ultrahigh quality factor Q and small mode volume, has witnessed remarkable progress [2–9] over the last few decades. On the basis of microcavities, these platforms show great potential in various applications such as ground-state cooling [10–16], entanglement [17–20], quantum state transfer [21–23], and nonreciprocity [24–27]. Among quantum information processing tasks, high-efficiency ground-state cooling promises great initialization and fidelity [21,28,29]. Several schemes have been proposed to realize the tremendous performance of ground-state cooling with various technologies [30–32]. With the increased phonon lifetimes and high frequency, Brillouin cavity optomechanics opens the possibility for macroscopic quantum control even at room temperature. Based on coherent light-sound coupling, stimulated Brillouin scattering has enabled high-efficiency laser cooling [32–35]. Furthermore, the Brillouin system with a large optomechanical coupling rate provides a rich avenue for quantum mechanical state control at the single-phonon and multiphonon levels, which offers practical optomechanical interfaces in hybrid quantum networks.

However, real applications of whispering gallery mode (WGM) optical microcavities face several limitations in their optomechanical cooling performance. The Q factors of both optical and mechanical modes are highly important, which has driven many efforts in precise engineering to achieve ultrahigh Q factors. Moreover, defects induced in the fabrication processes, such as deformed cavity geometry and scatters [36–39], are easily overlooked major constraints. These defects, even in subwavelength disorders, can lead to effective internal mode coupling [40] with undesirable modes, which cannot be eliminated using state-of-the-art approaches. This internal mode scattering forms a dark mode, which restrains the ultimate limits of phonon cooling. Backscattering between clockwise (CW) and counterclockwise (CCW) optical modes can hinder the application performance of radiation-pressure cavity optomechanics. The situation is even worse in a Brillouin scattering optomechanical system, when internal defect scattering occurs between the two degenerate Brillouin mechanical modes.

In this paper, we propose a compensatory cooling mechanism for a Brillouin scattering optomechanical system with exceptional points (EPs) [41–50]. By using EPs in both optical and mechanical modes, the limited cooling process is compensated effectively, and we can overcome the cooling rate and limit in virtual optomechanical devices with fabrication imperfections. The dual-EP system can be induced by two defects with specific relative angles. It actively manipulates the coupling strength of not only the optical modes but also the Brillouin phonon modes. When both the optical and the mechanical modes are at the EPs, the dark-mode effect vanishes. Our results provide tools for manipulating optomechanical interactions in multimode systems [42,44] and open possibilities for quantum state transfer and quantum interface protocols based on phonon cooling in quantum applications.

The remainder of this paper is organized as follows. In Sec. II we describe the Brillouin scattering optomechanical system. In Sec. III we analyze the optomechanical compensatory cooling. Conclusions are presented in Sec. IV.

*These authors contributed equally to this work.

†gllong@tsinghua.edu.cn

II. BRILLOUIN SCATTERING OPTOMECHANICAL SYSTEM

For a Brillouin scattering process, the Hamiltonian describing the optomechanical system with internal mode scattering is

$$H = \sum_j \Delta a_j^\dagger a_j + \sum_j \omega_m b_j^\dagger b_j + G(a_1^\dagger b_1 + b_1^\dagger a_1) + J(a_1^\dagger a_2 + a_2^\dagger a_1) + V(b_1^\dagger b_2 + b_2^\dagger b_1), \quad (1)$$

where $\hbar = 1$, a_j (b_j) denotes the optical (mechanical) mode with damping rate κ_o (γ_o), and $j = 1, 2$ denote the CW and CCW modes, respectively. Δ is the detuning between the optical frequency and pump laser, and G denotes the effective optomechanical strength. According to the Hamiltonian in Eq. (1), the cooling performance of the mechanical mode b_1 in the weak-coupling regime is limited by the internal mode scattering even for small J and V:

$$n_e = \frac{1 + C_{bb}}{1 + \frac{C_{ab}}{1+C_{aa}} + C_{bb}} \widetilde{n}_{th}. \quad (2)$$

Here, $\Delta = -\omega_m, C_{ab} = 4|G|^2/\gamma\kappa, C_{aa} = 4|J|^2/\kappa^2$, and $C_{bb} = 4|V|^2/\gamma^2$, where κ (γ) is the total optical (mechanical) loss with scattering [49]. In the calculation process, the photon occupation number in the environment is neglected because the optical resonant frequency is orders of magnitude higher. When $J = 0$ and $V = 0$, the system is in an ideal condition with the classical cooling limit $\frac{\widetilde{n}_{th}}{C_{ab}}$. However, in a real system with defects, internal coupling forms dark states, which hinder cooling via the different mechanisms shown in Eq. (2). For example, when only internal coupling exists between optical modes ($V = 0$), the interaction Hamiltonian can be rewritten in the form $\tilde{G}(a_1^\dagger b_B + b_B^\dagger a_1)$, in which the bright mode $b_B = (Gb_1 + Ja_2)/\tilde{G}$ is the hybridization of modes b_1 and a_2 with the coupling rate $\tilde{G} = \sqrt{|G|^2 + |J|^2}$. Because the dark mode $b_d = (Jb_1 - Ga_2)/\tilde{G}$ decouples from mode a_1, the cooling efficiency is suppressed. In this case, the steady-state phonon number n_e can be simplified under the conditions of a small J, $n_e = \frac{\widetilde{n}_{th}}{1+C_{ab}(1-2C_{aa})}$. It is clear that the deteriorated cooling mechanism originates from the decrescent optomechanical coupling rate induced by optical internal coupling. The steady phonon number increases owing to the dark state compared with the ideal optomechanical device, as shown in Fig. 1(b). This cooling suppression phenomenon imposes more restrictions on the cooling techniques and thermal bath temperature. To understand the evolution of the system in the optical dark mode, the master equation was applied. Figure 1(c) plots the dynamical cooling process with ideal (black line) and only optical scattering (blue line). Clearly, the suppressed optomechanical damping rate reduces the cooling speed, and the system requires more time to achieve a steady state. However, when the system suffers the coupling of optical modes $J = 0$, a dark state consisting of two mechanical modes emerges. In this case, the phonon occupation can be calculated, and the fundamental limit can be simplified as $n_e = \frac{1+C_{bb}}{C_{ab}}\widetilde{n}_{th}$. The dark state with two mechanical modes results in another heating channel for the system, which poses a fundamental limit for laser cooling in a virtual environment. The four-mode coupled system, described in Eq. (1), can be treated as a two-modes-coupled system with two effective mechanical thermal baths, shown in Fig. 1(a). The steady and dynamic phonon numbers of the system with both modes of scattering are plotted in Figs. 1(b) and 1(c), respectively.

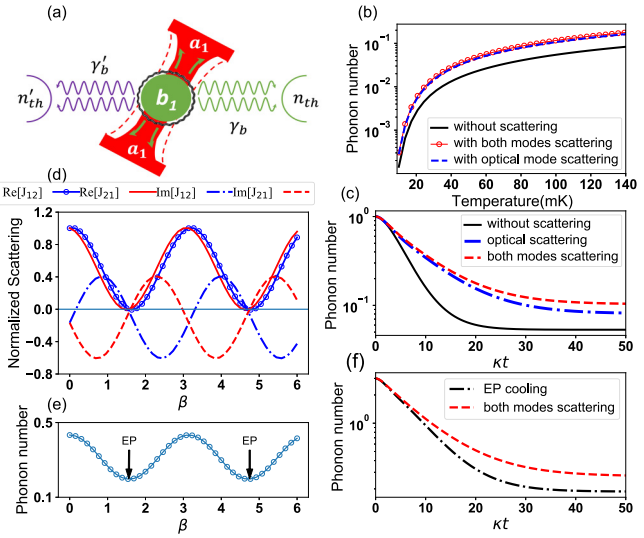

FIG. 1. (a) Schematic of the optomechanical system with decrescent optomechanical coupling rate and an external effective thermal bath. (b) The steady-state phonon number for different mode scattering strength with $\omega_m = 183$ MHz. (c) Dynamical evolution of the phonon number with internal modes coupling when the thermal temperature is 79.5 mK. (d) The elements J_{12}, J_{21} of the effective optical coupling and (e) the steady-state phonon number vs the the phase β with $V = (0.35 - 0.1i)\gamma_o$, $\widetilde{n}_{th} = 3$, $J_1 = J_2 = (0.502 - 0.063i)\kappa_o$. (f) The time evolution of the phonon number when both optical and mechanical modes of the undriven system are prepared at EPs. The other parameters are $\kappa_o = 1$ MHz, $J = (0.5 - 0.1i)\kappa_o$, $\gamma_o = 0.01\kappa_o$, $G = 0.24\kappa_o$.

To achieve ground-state cooling, suppressing thermal heating and enhancing the optomechanical damping rate should be employed simultaneously. In contrast to previous straightforward techniques that aim to eliminate scattering, we employ active scattering control to increase the optomechanical damping rate and suppress the heating swap between the two mechanical modes. In particular, when an undriven system is prepared on the EPs, dark-mode effects can be eliminated. In this case, the interaction Hamiltonian of the undriven system is

$$H_u = J_{12}c_1^\dagger c_2 + J_{21}c_2^\dagger c_1 + V_{12}b_1^\dagger b_2 + V_{21}b_2^\dagger b_1. \quad (3)$$

For the optical modes, $J_{12} = J + J_1 e^{2i\beta}$ ($J_{21} = J + J_2 e^{-2i\beta}$) is the tunable coupling rate after actively controlling scattering with J_1 (J_2). Figure 1(d) demonstrates the tunability of the optical mode coupling strength, where all the elements of J_{12} and J_{21} vanish for a certain phase β. The best cooling performance was achieved when the undriven system was at the optical EPs, as shown in Fig. 1(e). At the same time, V_{12} (V_{21}) has the same form as J_{12} (J_{21}), and the energy scattering of mechanical modes can be tuned to achieve mechanical EPs through V_1 and V_2. When both the optical and mechanical modes of the undriven system are prepared at the EPs by

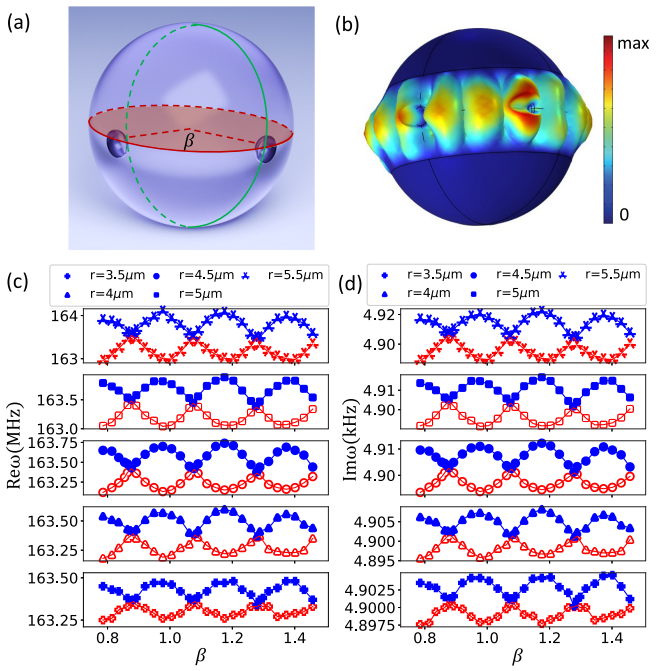

FIG. 2. (a) Diagram of a microresonator with two defects; the relative angle between the two defects is β. (b) Simulation result of the typical mechanical vibration characterized by an eigenfrequency around 163 MHz. (c) and (d) Real and imaginary parts of the mechanical eigenvalues with different defect sizes vs the relative angle β. The radius of the resonator $R = 60$ μm.

setting $V_1 = V_2 = (0.35 - 0.068i)\gamma_o$, the cooling efficiency is further optimized, as shown in Fig. 1(f).

III. OPTOMECHANICAL COMPENSATORY COOLING

We take advantage of defects to form EPs and realize a more effective cooling device containing the main features of the toy model where the coherent control of mode scattering is applied. The universal design is illustrated in Fig. 2(a). Two defects with a relative angle β are introduced to form EPs in the resonator, which consists of an optical mode pair (a_1, a_2) with degenerate frequency ω_a and a mechanical mode pair (b_1, b_2) with degenerate frequency ω_m. We implemented finite-element simulations of defective resonators with different defect sizes with the aid of COMSOL MULTIPHYSICS software. The material of the resonator is silicon dioxide, which is in the material library, and the other components are filled with air. The typical simulation result of the Brillouin mode and mechanical vibration distributed around the equatorial plane of the resonator with azimuthal number $m_b = 8$ is shown in Fig. 2(b). It is worth noting that this set of parameters serves only as an example. In principle, there is no limitation regarding the resonator size, defect size, wavelength, or refractive indices. Figures 2(c) and 2(d) demonstrate the real and imaginary parts of the mechanical eigenvalues, which correspond to the frequencies and linewidths, with different defect sizes. It can be found that the frequencies and linewidths of the Brillouin mode pair share similar periodic behavior as β changes, with the period π/m_b.

Figures 3(a) and 3(b) denote the real parts and imaginary parts of differences for different defect sizes. In addition, the

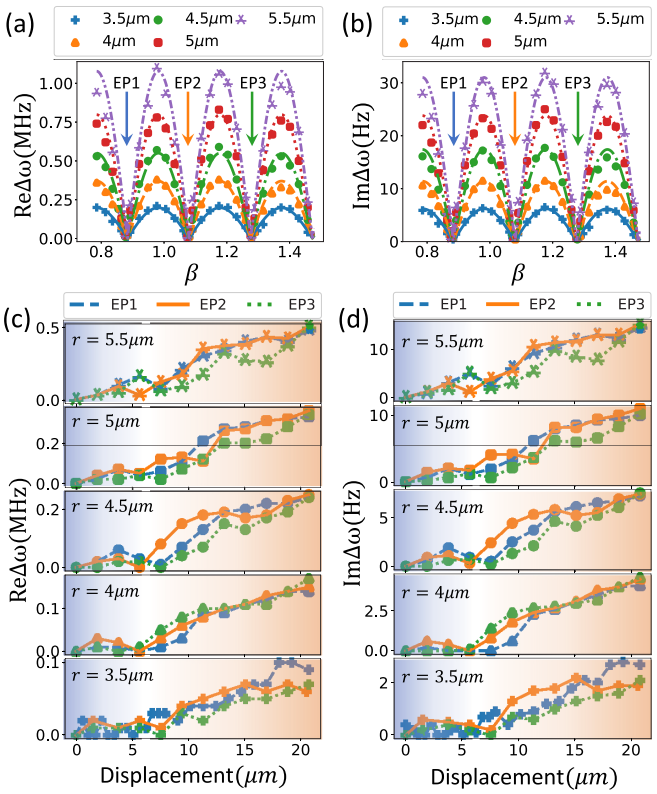

FIG. 3. (a) and (b) Real parts and imaginary parts of differences of the mechanical eigenvalues vs the relative angle for different defect sizes. (c) and (d) Real parts and imaginary parts of differences of the mechanical eigenvalues vs the displacement along the green line in Fig. 2(a) at three EPs for different defect sizes. The radius of the resonator $R = 60$ μm. The mode coupling rates of the defect sizes 3.5, 4, 4.5, 5, and 5.5 μm correspond to $\{e_{b1}, e_{b2}\} = \{5 \times 10^4 - 1.5i, 4.9 \times 10^4 - 1.6i\}$ Hz, $\{9.3 \times 10^4 - 2.8i, 9.2 \times 10^4 - 2.9i\}$ Hz, $\{13.8 \times 10^4 - 4.3i, 13.7 \times 10^4 - 4.4i\}$ Hz, $\{20 \times 10^4 - 5.9i, 19.9 \times 10^4 - 6i\}$ Hz, and $\{27 \times 10^4 - 7.7i, 26.9 \times 10^4 - 7.8i\}$ Hz, respectively.

differences $\mathrm{Re}\Delta\omega$ and $\mathrm{Im}\Delta\omega$ change periodically with β and have the same period π/m_b, $\Delta\omega = 2\sqrt{e_{b1}^2 + e_{b2}^2 + 2e_{b1}e_{b2}\cos(2m_b\beta)}$. e_{b1} and e_{b2} are the mode coupling rates induced by defects 1 and 2, respectively. Furthermore, the larger the number of defects, the larger is the maximum value of the difference. The simulation results are in good agreement with the qualitative analysis. Both the coupling coefficients, J_{b1} and J_{b2}, have an exponential factor $2im_b\beta$, which indicates a period equal to π/m_b. The effect of defects on the Brillouin mode pair is restricted by their size. Small defects have a limited impact on the mode, causing a slight difference between the real and imaginary parts. At specific points, that is, 0.876, 1.077, and 1.278, the real and imaginary parts of the Brillouin mode pair coalesce simultaneously; these points are called EPs. To test the robustness of the defective system, the position of defect 2 was applied to a displacement from the equatorial plane along the green line shown in Fig. 2(a). For different defect sizes, the differences between the real and imaginary parts at the three EPs' angles versus displacement are shown in Figs. 3(c) and 3(d). It can be observed that at some displacement range ($\leqslant 5$ μm), the EPs are maintained, and the system shows robustness with the position displacement along the direction

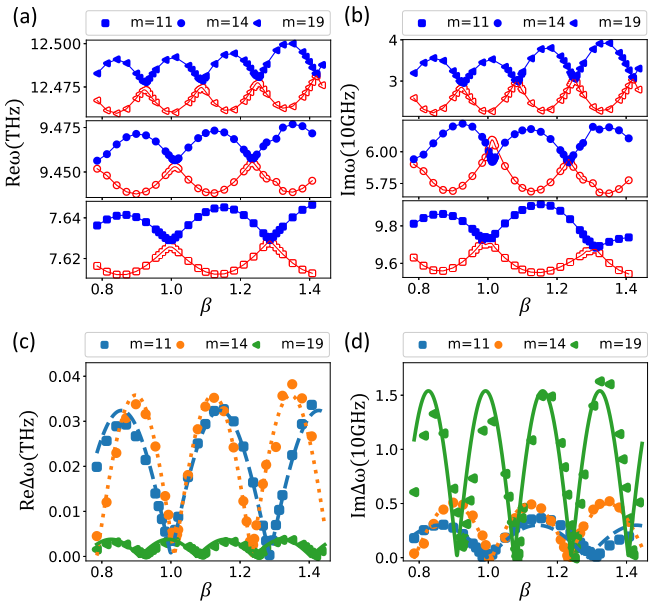

FIG. 4. (a) and (b) Real and imaginary parts of the optical eigenvalues with different azimuthal mode numbers vs the relative angle β. (c) and (d) Real parts and imaginary parts of differences of the optical eigenvalues vs the relative angle β with different azimuthal mode numbers. Dots in this figure are simulation results, whereas lines in (c) and (d) are theoretical curves. The radius of the cavity is $R = 60$ μm, and the radius of the defects is $r = 4.5$ μm. The mode coupling rates of $m = 11, 14$, and 19 correspond to $\{e_{a1}, e_{a2}\} = \{8.3 \times 10^9 - 7 \times 10^8 i, 7.9 \times 10^9 - 8 \times 10^8 i\}$ Hz, $\{9 \times 10^9 - 1.2 \times 10^9 i, 8.9 \times 10^9 - 1.3 \times 10^9 i\}$ Hz, and $\{1 \times 10^9 - 3.8 \times 10^9 i, 0.9 \times 10^9 - 3.9 \times 10^9 i\}$ Hz, respectively.

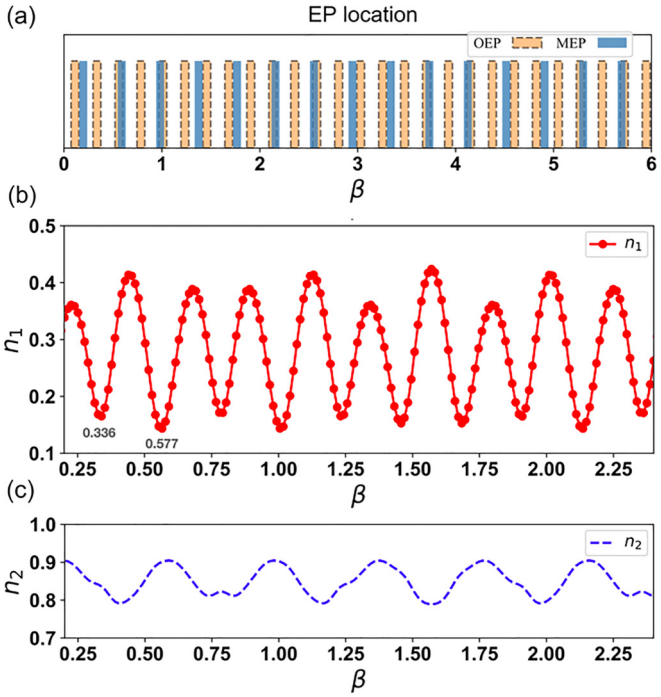

FIG. 5. Normalized steady phonon number of two mechanical modes vs phase β. (a) OEPs and MEPs emerge for different defect locations. (b) and (c) plot the normalized occupancy of modes b_1 and b_2 with optomechanical coupling strength $G/\kappa_o = 0.155$, $m_a = 14$, and $m_b = 8$. The other parameters are the same as in Fig. 1.

perpendicular to the equatorial plane. Furthermore, the system exhibits higher robustness for smaller defect sizes.

The proposed scheme also works to reach the optical EP, and the visualized mode control upon defect engineering is shown in Fig. 4. The azimuthal numbers of the optical modes considered herein are $m_a = 11$, 14, and 19. Figures 4(a) and 4(b) demonstrate the real and imaginary parts of the optical eigenvalues with different azimuthal numbers as β varies. The frequencies and linewidths of the optical modes have the same period π/m_c, as predicted by the theoretical analysis. In addition, there are EPs for the optical mode pair at which the frequencies and linewidths coalesce simultaneously, such as $\beta = 1.419$ in the $m_a = 19$ case, for example. To demonstrate the presence or absence of EPs, Figs. 4(c) and 4(d) imply the difference between the real parts and the imaginary parts of the optical modes.

We now study the cooling performance of the mechanical resonator using the optomechanical system described above. To calculate the evolution for all modes of the optomechanical system, we should consider all dissipations induced by the two defects. To demonstrate the impact of defects on cooling, we calculated the steady solution of the two mechanical modes for various angles of β, as shown in Fig. 5. Because the azimuthal numbers of the optical and mechanical modes are different, the periods of the mechanical exceptional point (MEP) and optical exceptional point (OEP) are different in Fig. 5(a). The MEP and OEP occurring at different angles β can affect phonon occupancy. The plots show that both modes b_1 and b_2, represented by the red line with dots and the blue dashed line, respectively, are cooled when the relative angle changes. For the mechanical mode b_1, the steady phonon number also demonstrates a periodic variation. In general, the period is $\frac{m\pi}{m_a m_b}$, where m is the least common multiple of m_a and m_b; in this case, it is $\frac{\pi}{2}$. When $\beta = 0.336$, the phonon number decreased to its local minimum for the cooled mode b_1. However, the mechanical modes still couple with each other, resulting in the suppression of cooling for b_1. When $\beta = 0.577$, the undriven optical modes and mechanical modes are prepared at their EP, and the phonon number of the cooled mode b_1 reaches the global minimum. The phonon number of b_2 reached the global maximum, indicating that the cooling of b_2 was efficiently suppressed. The dark-mode effect was completely inhibited, and the phonon number reached its cooling limit.

IV. CONCLUSION

In this paper, we proposed a compensatory cooling mechanism for a Brillouin scattering optomechanical system with EPs. When those are used in both optical and mechanical modes, the limited cooling process is compensated effectively, as EPs can suppress thermal heating and enhance the optomechanical damping rate simultaneously. The dual-EP system can be induced by two defects with specific relative angles, and it actively and concurrently manipulates the coupling strength of the optical and Brillouin phonon modes. This approach can overcome the ultimate limits of phonon cooling

induced by mode scattering in both real and fundamental applications.

ACKNOWLEDGMENTS

This work was supported by the National Natural Science Foundation of China (Grants No. 61727801 and No. 62131002), National Key Research and Development Program of China (Grant No. 2017YFA0303700), Key Research and Development Program of Guangdong Province (Grant No. 2018B030325002), Beijing Advanced Innovation Center for Future Chips (ICFC), and Tsinghua University Initiative Scientific Research Program.

[1] M. Aspelmeyer, T. J. Kippenberg, and F. Marquardt, Rev. Mod. Phys. **86**, 1391 (2014).
[2] M. Forsch, R. Stockill, A. Wallucks, I. Marinković, C. Gärtner, R. A. Norte, F. van Otten, A. Fiore, K. Srinivasan, and S. Gröblacher, Nat. Phys. **16**, 69 (2020).
[3] C. Ockeloen-Korppi, E. Damskägg, J.-M. Pirkkalainen, M. Asjad, A. Clerk, F. Massel, M. Woolley, and M. Sillanpää, Nature (London) **556**, 478 (2018).
[4] R. Riedinger, A. Wallucks, I. Marinković, C. Löschnauer, M. Aspelmeyer, S. Hong, and S. Gröblacher, Nature (London) **556**, 473 (2018).
[5] A. Bienfait, K. J. Satzinger, Y. Zhong, H.-S. Chang, M.-H. Chou, C. R. Conner, É. Dumur, J. Grebel, G. A. Peairs, R. G. Povey, and A. N. Cleland, Science **364**, 368 (2019).
[6] C. Dong, V. Fiore, M. C. Kuzyk, and H. Wang, Science **338**, 1609 (2012).
[7] Y.-C. Liu, Y.-F. Xiao, X. Luan, and C. W. Wong, Phys. Rev. Lett. **110**, 153606 (2013).
[8] D. J. Wilson, V. Sudhir, N. Piro, R. Schilling, A. Ghadimi, and T. J. Kippenberg, Nature (London) **524**, 325 (2015).
[9] W.-L. Xu, Y.-P. Gao, C. Cao, T.-J. Wang, and C. Wang, Phys. Rev. A **102**, 043519 (2020).
[10] H. Xu, L. Jiang, A. A. Clerk, and J. G. E. Harris, Nature (London) **568**, 65 (2019).
[11] I. Wilson-Rae, N. Nooshi, W. Zwerger, and T. J. Kippenberg, Phys. Rev. Lett. **99**, 093901 (2007).
[12] F. Marquardt, J. P. Chen, A. A. Clerk, and S. M. Girvin, Phys. Rev. Lett. **99**, 093902 (2007).
[13] D.-G. Lai, F. Zou, B.-P. Hou, Y.-F. Xiao, and J.-Q. Liao, Phys. Rev. A **98**, 023860 (2018).
[14] J.-H. Gan, Y.-C. Liu, C. Lu, X. Wang, M. K. Tey, and L. You, Laser Photonics Rev. **13**, 1900120 (2019).
[15] J.-Y. Liu, W. Liu, D. Xu, J.-C. Shi, H. Xu, Q. Gong, and Y.-F. Xiao, Phys. Rev. A **105**, 053518 (2022).
[16] K.-W. Xiao, A. Xiong, N. Zhao, and Z.-q. Yin, Quantum Eng. **3**, e62 (2021).
[17] D. Vitali, S. Gigan, A. Ferreira, H. R. Böhm, P. Tombesi, A. Guerreiro, V. Vedral, A. Zeilinger, and M. Aspelmeyer, Phys. Rev. Lett. **98**, 030405 (2007).
[18] J.-Q. Liao and L. Tian, Phys. Rev. Lett. **116**, 163602 (2016).
[19] C. Zhong, X. Han, H. X. Tang, and L. Jiang, Phys. Rev. A **101**, 032345 (2020).
[20] H. Flayac and V. Savona, Phys. Rev. Lett. **113**, 143603 (2014).
[21] K. Stannigel, P. Rabl, A. S. Sørensen, P. Zoller, and M. D. Lukin, Phys. Rev. Lett. **105**, 220501 (2010).
[22] Y.-D. Wang and A. A. Clerk, Phys. Rev. Lett. **108**, 153603 (2012).
[23] L. Tian, Phys. Rev. Lett. **108**, 153604 (2012).
[24] L. Tang, J. Tang, M. Chen, F. Nori, M. Xiao, and K. Xia, Phys. Rev. Lett. **128**, 083604 (2022).
[25] X.-W. Xu, L. N. Song, Q. Zheng, Z. H. Wang, and Y. Li, Phys. Rev. A **98**, 063845 (2018).
[26] D.-W. Zhang, L.-L. Zheng, C. You, C.-S. Hu, Y. Wu, and X.-Y. Lü, Phys. Rev. A **104**, 033522 (2021).
[27] Y. Jiao, C.-H. Bai, D.-Y. Wang, S. Zhang, and H.-F. Wang, Quantum Eng. **2**, e39 (2020).
[28] K. Stannigel, P. Komar, S. J. M. Habraken, S. D. Bennett, M. D. Lukin, P. Zoller, and P. Rabl, Phys. Rev. Lett. **109**, 013603 (2012).
[29] R. Riedinger, S. Hong, R. A. Norte, J. A. Slater, J. Shang, A. G. Krause, V. Anant, M. Aspelmeyer, and S. Gröblacher, Nature (London) **530**, 313 (2016).
[30] O. Arcizet, P.-F. Cohadon, T. Briant, M. Pinard, and A. Heidmann, Nature (London) **444**, 71 (2006).
[31] Y.-S. Park and H. Wang, Nat. Phys. **5**, 489 (2009).
[32] G. Bahl, M. Tomes, F. Marquardt, and T. Carmon, Nat. Phys. **8**, 203 (2012).
[33] S. Kim, X. Xu, J. M. Taylor, and G. Bahl, Nat. Commun. **8**, 205 (2017).
[34] N. T. Otterstrom, R. O. Behunin, E. A. Kittlaus, and P. T. Rakich, Phys. Rev. X **8**, 041034 (2018).
[35] Y.-C. Chen, S. Kim, and G. Bahl, New J. Phys. **18**, 115004 (2016).
[36] S. Kim, J. M. Taylor, and G. Bahl, Optica **6**, 1016 (2019).
[37] J. Nöckel, A. Stone, and R. Chang, Opt. Lett. **19**, 1693 (1994).
[38] H.-H. Yu, C.-H. Yi, and C.-M. Kim, Opt. Express **23**, 11054 (2015).
[39] A. G. Griffith, R. K. Lau, J. Cardenas, Y. Okawachi, A. Mohanty, R. Fain, Y. H. D. Lee, M. Yu, C. T. Phare, C. B. Poitras, A. L. Gaeta, and M. Lipson, Nat. Commun. **6**, 6299 (2015).
[40] A. Mazzei, S. Götzinger, L. des S. Menezes, G. Zumofen, O. Benson, and V. Sandoghdar, Phys. Rev. Lett. **99**, 173603 (2007).
[41] W. Chen, Ş. K. Özdemir, G. Zhao, J. Wiersig, and L. Yang, Nature (London) **548**, 192 (2017).
[42] J. Wiersig, Phys. Rev. Lett. **112**, 203901 (2014).
[43] M. De Carlo, F. De Leonardis, R. A. Soref, L. Colatorti, and V. M. Passaro, Sensors **22**, 3977 (2022).
[44] H. Xu, D. Mason, L. Jiang, and J. Harris, Nature (London) **537**, 80 (2016).
[45] G.-Q. Qin, R.-R. Xie, H. Zhang, Y.-Q. Hu, M. Wang, G.-Q. Li, H. Xu, F. Lei, D. Ruan, and G.-L. Long, Laser Photonics Rev. **15**, 2000569 (2021).
[46] H. Jiang, W. Zhang, G. Lu, L. Ye, H. Lin, J. Tang, Z. Xue, Z. Li, H. Xu, and Q. Gong, Photonics Res. **10**, 557 (2022).

[47] K. Ding, C. Fang, and G. Ma, Nat. Rev. Phys. **4**, 745 (2022).
[48] J. Zhang, B. Peng, Ş. K. Özdemir, K. Pichler, D. O. Krimer, G. Zhao, F. Nori, Y.-x. Liu, S. Rotter, and L. Yang, Nat. Photonics **12**, 479 (2018).
[49] H. Lü, C. Wang, L. Yang, and H. Jing, Phys. Rev. Appl. **10**, 014006 (2018).
[50] X. Mao, G.-Q. Qin, H. Yang, H. Zhang, M. Wang, and G.-L. Long, New J. Phys. **22**, 093009 (2020).